Strategies for enhanced accuracy in 1D fluid simulation of Hall thruster IEPC-2024-377

Federico Petronio, Alejandro Alvarez Laguna, Anne Bourdon, Pascal Chabert, Benjamin Esteves

Strategies for enhanced accuracy in 1D fluid simulation of Hall thruster

IEPC-2024-377

Presented at the 38th International Electric Propulsion Conference, Toulouse, France
June 23-28, 2024

Federico Petronio[*], Alejandro Alvarez Laguna[†], Anne Bourdon[‡], and Pascal Chabert[§]
Laboratoire de Physique des Plasmas (LPP), Ecole Polytechnique, CNRS, Institut Polytechnique de Paris, France
COMHET laboratory
Benjamin Esteves[¶]
Safran Spacecraft Propulsion (SSP), COMHET laboratory[‖]

Hall Thrusters (HTs) are technologically advanced systems that are nowadays largely used for space propulsion. The understanding of the physics of these devices is crucial for their optimization. In this work, we present a fluid analytical model for describing the electron transport in a HT. By using the results of a hybrid simulation (i.e. particle-in-cell charged species and fluid neutrals), we challenge this model. We show how the axial anomalous transport can be correlated with the plasma instabilities, without inquiring about their origin. In particular, we discuss the opportunity and the limits of using the anomalous collisional frequency as a proxy for the anomalous transport. Despite the numerous efforts in this sense made by the community, we show that the approach of artificially increasing the collision frequency is not the best one, in a data driven approach. We eventually propose a different method, to be used in fluid models, to take into account the oscillations or turbulence of the plasma inducing the anomalous transport. This method has been implemented in a 1D purely axial fluid model to take into account the anomalous transport generated by the azimuthal electron motion. The preliminary results of this model are presented and discussed.

[*]Simulation pole manager, COMHET laboratory, federico.petronio@lpp.polytechnique.fr.
[†]Chargé de Recherche, CNRS, alejandro.alvarez-laguna@lpp.polytechnique.fr.
[‡]Directeur de Recherche, CNRS, anne.bourdon@lpp.polytechnique.fr.
[§]Directeur de Recherche, CNRS, pascal.chabert@lpp.polytechnique.fr.
[¶]Alternative propellants pole manager, COMHET laboratory, benjamin.esteves@safrangroup.com.
[‖]COMHET: a joint laboratory for the study of Hall Effect Thrusters, an École Polytechnique, CNRS and Safran Electronics & Defense joint venture

Nomenclature

E_x	= Electric field in the axial direction
K_{iz}	= Ionization rate coefficient
T_e	= Electron temperature
e	= Elementary charge
m_i	= Ion mass
n	= Plasma density
n_g	= Electron Cyclotron Drift Instability
$v_{e,x}$ and $v_{e,y}$	= Electron axial and azimuthal velocities
$v_{i,x}$ and $v_{i,y}$	= Ion axial and azimuthal velocities
x, y	= Axial and azimuthal directions
Ψ	= Drift-dependent velocity term
γ_i	= Energy loss parameter
$\mathbf{E}$	= Electric field
$\mathbf{J_e}$	= Electron current density
$\mathbf{P_e}$	= Electron pressure tensor
$\mathbf{q}_e$	= Electron heat-flux vector
$\mathbf{v}_D$	= Diamagnetic drift velocity
$\mathbf{v}_E$	= Electron $\mathbf{E} \times \mathbf{B}$ velocity
$\mu_\perp$	= Perpendicular mobility
ν	= Momentum transfer collision frequency
ν_{iw}	= Ion-wall collision frequency
ω_{ce}	= Electron cyclotron frequency
ϕ_{iz}	= Ionization potential

I. Introduction

Hall Thrusters (HTs) are currently one of the most advanced and used technologies in the field of electric propulsion.[1] Although those devices have been successfully used for several decades, further development is still required to improve their performances and efficiently develop the new generation of thrusters.

A HT device consists of a ring-shaped chamber into which a gas, usually xenon or krypton, is injected. This annular channel is open at one end, while the other end serves as the anode. An external grounded cathode provides electrons that are attracted to the channel by the strong positive electric bias of the anode. A static magnetic field directed radially, combined with the axial electric field generated by the potential difference between the anode and cathode, accelerates the electrons in the azimuthal direction, causing them to orbit inside the ring. This movement is known as the $\mathbf{E} \times \mathbf{B}$ drift. The $\mathbf{E} \times \mathbf{B}$ drift increases the electron residence time inside the chamber, which enhances the ionization of the gas and the creation of plasma. The electrons are then collected by the anode, while the ions are accelerated in the opposite direction, creating thrust.

To facilitate the development of new thrusters and to enhance the understanding of the physics within these devices, the scientific community has developed several models and simulation tools. These simulation tools can be broadly categorized into two major families. The first family consists of kinetic simulations, typically employing the Particle-in-Cell (PIC) approach. This method represents plasma dynamics through the use of macro-particles and is particularly effective for investigating plasma instabilities and turbulence. The second family includes fluid simulations, which are based on fluid equations and are primarily utilized to examine the global behavior of the plasma. A significant advantage of fluid simulations is their lower computational cost compared to kinetic simulations. However, standard fluid simulations of HTs have failed to reproduce certain experimental results accurately. The origin of this discrepancy has been identified as the lack of anomalous transport (i.e. the abnormal electron diffusion towards the anode) in fluid models.[2]

For this reason, since the first attempts of simulating the HT discharge,[3–6] the researchers have included in their models some mechanisms to take into account the anomalous electron diffusion along the thruster axis. In these works, the anomalous electron transport was usually modeled by artificially increasing the electron collision frequency. Although the origin of this phenomenon was not completely clear, the community has agreed on the need to include this type of transport in fluid simulations to successfully reproduce the experimental results.[2]

Despite the numerous achievements in understanding the anomalous transport from theoretical point of view[7–10] and by the use of kinetic simulations,[11–13] the way of modeling this transport in fluid models is still a matter of debate[14] and remained semi-empirical. Thus, the most common way to account for the anomalous transport remains to artificially increase the electron collision frequency.[15–21] Although this approach has enabled the community to successfully reproduce some experimental results, it has not proven to be robust. This is because it necessitates iterative adjustments between simulation outcomes and empirical parameters to align the model with experimental data. Furthermore, we will prove in this work that artificially increasing the collision frequency requires careful consideration. Our goal is to develop a model capable of replicating experimental results without relying on empirical parameters specific to each thruster model.

In this work, we first analyze electron transport in a HT using fluid theory. Specifically, we demonstrate how density and electric field fluctuations influence electron transport within a fluid model. We then introduce the hybrid code LPPic, which is utilized in the subsequent section to challenge the fluid model described initially. Later, we explore the feasibility of implementing this model in a 1D fluid code. Preliminary results of this implementation are presented. Eventually, we discuss potential future developments.

II. Analytical model

In this section, we will describe a 1D (i.e. along the thruster axis) fluid analytical model for a HT. The model is based on a simplified version of the work from Barral and Ahedo,[16] already used in Refs. 22,23. The model solves a quasi-neutral system composed of gas and plasma continuity equations, momentum equation

for ions, and energy equation for electrons:

$$\frac{\partial n_g}{\partial t} + \nabla \cdot (n_g v_g) = - n_g n K_{iz} + \nu_{iw} n, \tag{1}$$

$$\frac{\partial n}{\partial t} + \nabla \cdot (n v_{i,x}) = + n_g n K_{iz} - \nu_{iw} n, \tag{2}$$

$$\frac{\partial (n v_{i,x})}{\partial t} + \frac{\partial \left(n v_{i,x}^2\right)}{\partial x} = n_g n v_g K_{iz} - \nu_{iw} n v_{i,x} + \frac{e}{m_i} n E_x, \tag{3}$$

$$\frac{\partial}{\partial t}\left(\frac{1}{2} m n v_e^2 + \frac{3}{2} P_e\right) + \nabla \cdot \left[\left(\frac{1}{2} m n v_e^2 + \frac{3}{2} P_e\right) \mathbf{v_e} + \mathbf{P_e} \cdot \mathbf{v_e} + \mathbf{q}_e\right] - \mathbf{E} \cdot \mathbf{J_e} = -n_g n \gamma_i \phi_{iz} K_{iz} - \nu_{iw} n T_e, \tag{4}$$

where n_g is the gas density, v_g is the fixed gas speed, n is the plasma density, $v_{i,x}$ is the ion axial velocity, K_{iz} is the ionization rate coefficient, ν_{iw} is the ion-wall collision frequency, m_i is the ion mass, E_x is the electric field in the axial direction, e is the elementary charge, T_e is the electron temperature, $\mathbf{v_e}$ is the electron velocity, $\mathbf{P_e}$ is the electron pressure tensor, $\mathbf{E}$ is the electric field, $\mathbf{q}_e$ is the electron heat-flux vector, $\mathbf{J_e}$ is the electron current density, γ_i is an energy loss parameter, and ϕ_{iz} is the ionization potential.

Now, let us focus on the electron transport. Starting from the momentum equation from electrons in which we neglected inertia terms, we can write in vectorial form:[24]

$$\mathbf{v}_\perp = -\mu_\perp \left(\mathbf{E} + \nabla (n k_B T_e)/n\right) + \frac{\mathbf{v}_E + \mathbf{v}_D}{1 + \nu^2/\omega_{ce}^2}, \tag{5}$$

where, $\mathbf{v}_\perp$ is the perpendicular (to the magnetic field) velocity of the electrons, $\mu_\perp$ is the perpendicular mobility, $\mathbf{v}_E$ is the electron $\mathbf{E} \times \mathbf{B}$ velocity, $\mathbf{v}_D$ is the diamagnetic drift velocity, ν is the momentum transfer collision frequency and $\omega_{ce} = eB/m_e$ is the electron cyclotron frequency and m_e is the electron mass. In the following, we will also deal with the electron thermal pressure, defined as $P_e = n k_B T_e$, with k_B the Boltzmann constant. The symbol $\mathbf{B}$ represents the magnetic field vector. The electron mobility coefficient in the transverse direction (i.e. perpendicular to the magnetic field) can be expressed as

$$\mu_\perp = \frac{e/m_e \nu}{1 + \omega_{ce}^2/\nu^2},$$

In our conditions, as we will see, one can approximate the mobility as

$$\mu_\perp \approx \frac{\nu m_e}{e B^2}. \tag{6}$$

The electron $\mathbf{E} \times \mathbf{B}$ velocity and the diamagnetic drift velocity are given by

$$\mathbf{v}_E = \frac{\mathbf{E} \times \mathbf{B}}{B^2}, \tag{7}$$

$$\mathbf{v}_D = \frac{\nabla (n k_B T_e) \times \mathbf{B}}{n e B^2}, \tag{8}$$

respectively.

The components of Eq. (5) along the axial direction (i.e. x) and along the azimuthal direction (i.e. y), read

$$n v_{e,x,y} = -\mu_\perp (n E_{y,x} + \partial_{y,x} (n k_B T_e)) + n \Psi_{x,y}, \tag{9}$$

where we introduced the drift-dependent terms as Ψ-flux:

$$n \Psi_{x,y} \doteq \frac{n E_{y,x}/B + \partial_{y,x} (n k_B T_e)/B}{1 + \nu^2/\omega_{ce}^2}.$$

One should notice that within the Ψ-flux the azimuthal motion depends on the electric field in the axial direction and on the pressure gradient along the axial direction and vice versa.

We can then write the electric field in the axial direction, from Eq. (9) as

$$E_x = -\frac{\partial_x (n T_e)}{e n} - \frac{n v_{e,x} - n \Psi_x}{n \mu_\perp}. \tag{10}$$

If we integrate Eq. (10) along the axial direction between 0 and L, we get the current density inside the thruster as

$$\frac{I_0}{eA_0} = \frac{V(0) + \int_0^L (\partial_x(nk_BT_e)/n + (nv_{i,x} - n\Psi_x)/n\mu_\perp)\, dx}{\int_0^L 1/n\mu_\perp dx},$$

with I_0 the discharge current, A_0 the cross-sectional area of the HT, $V(0)$ the potential at the entrance of the HT, and L the anode/cathode distance.

The momentum equation along x for the ions, c.f. Eq. (3), can be rewritten, using Eq. (10), as

$$\frac{\partial(nv_{i,x})}{\partial t} + \frac{\partial}{\partial x}\left(nv_{i,x}^2 + n\frac{T_e}{m_i}\right) = n_g n v_g K_{iz} - \nu_{iw} n v_{i,x} - \frac{m_e\omega_{ce}^2}{m_i\nu}(nv_{e,x} - \langle n\Psi_x\rangle_y). \tag{11}$$

In the previous expression, we considered the azimuthal average of the Ψ-flux term, i.e. $\langle n\Psi_x\rangle_y$.

Considering the Joule-heating term $\mathbf{E}\cdot\mathbf{J}_e$ in the electron energy equation, we have

$$\mathbf{E}\cdot\mathbf{J}_e = -en\mathbf{E}\cdot\mathbf{v}_e = -en(E_x v_{e,x} + E_y v_{e,y}).$$

By averaging azimuthally, we get

$$\langle\mathbf{E}\cdot\mathbf{J}_e\rangle_y = -enE_x\left(v_{e,x} + \frac{\langle nE_y\rangle_y}{nB}\right) - \frac{\langle nE_y\rangle_y}{nB}\partial_x P_{e,x},$$

where we used that

$$v_{e,y} \approx (E_x + \partial_x P_{e,x}/en)/B. \tag{12}$$

This approximation will be verified in the next section. Then, Eq. (4), neglecting the heat-flux, can be written as

$$\frac{\partial}{\partial t}\left(\frac{3}{2}P_{e,x}\right) + \frac{\partial}{\partial x}\left(\frac{5}{2}P_{e,x}v_{e,x}\right) = \frac{\partial P_e}{\partial x}v_{e,x} + \frac{nv_{e,x} - \langle n\Psi_x\rangle_y}{n\mu_\perp}nv_{e,x} + \frac{nv_{e,x} - \langle n\Psi_x\rangle_y}{n\mu_\perp}\frac{\langle nE_y\rangle_y}{nB} - n_g n\gamma_i\phi_{iz}K_{iz} - \nu_{iw}nT_e.$$

Considering that

$$\langle n\Psi_x\rangle_y \approx \left\langle \frac{nE_y/B + \partial_y(nk_BT_e)/B}{1+\nu^2/\omega_{ce}^2}\right\rangle_y \approx \frac{\langle\delta n\delta E_y\rangle_y}{B}. \tag{13}$$

we can write

$$\frac{\partial}{\partial t}\left(\frac{3}{2}P_{e,x}\right) + \frac{\partial}{\partial x}\left(\frac{5}{2}P_{e,x}v_{e,x}\right) = \frac{\partial P_e}{\partial x}v_{e,x} + \frac{m_e\omega_{ce}^2 n}{\nu}\left(v_{e,x} - \frac{\langle\delta n\delta E_y\rangle_y}{nB}\right)^2 - n_g n\gamma_i\phi_{iz}K_{iz} - \nu_{iw}nT_e. \tag{14}$$

If we neglect the correlation term, Eq. (14) is the same electron energy conservation equation used in Ref. 23. The approximation in Eq. (13) will be analyzed in the next section.

If we look at the two equations 11 and 14, we can directly see the effect of the correlation of the electric field and density oscillations on the electron transport. This approach shows that the use of an artificial collision frequency cannot be easily linked to the anomalous (instability-induced) electron transport, when threated in this way. Even if we had a theory that perfectly describes the amplitude and frequency of the oscillations: no collision frequency can satisfy at the same time equations 11 and 14.

III. Hybrid simulation setup

The kinetic simulation to verify the theory discussed in Section II has been performed using a well-established hybrid (i.e. PIC/Monte-Carlo-Collision (MCC) charged species and fluid neutrals) code, LP-Pic.[25,26] This code is a 2D-3V electrostatic code that here is used to simulate the axial-azimuthal plane of a HT. The code considers electrons and singly charged ions, while the neutral background dynamics is

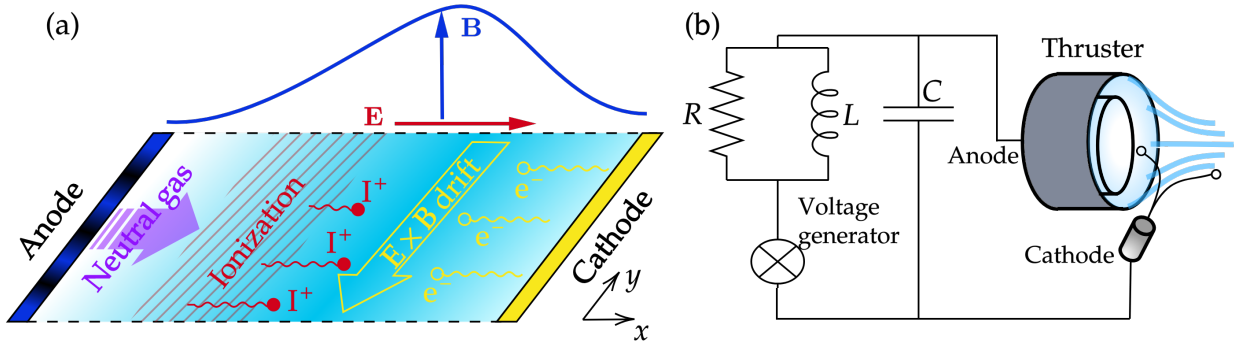

Figure 1. (a) Axial-azimuthal simulation domain used in LPPic hybrid simulations. (b) Scheme of the electrical circuit modeled in the simulation. Adapted from 30.

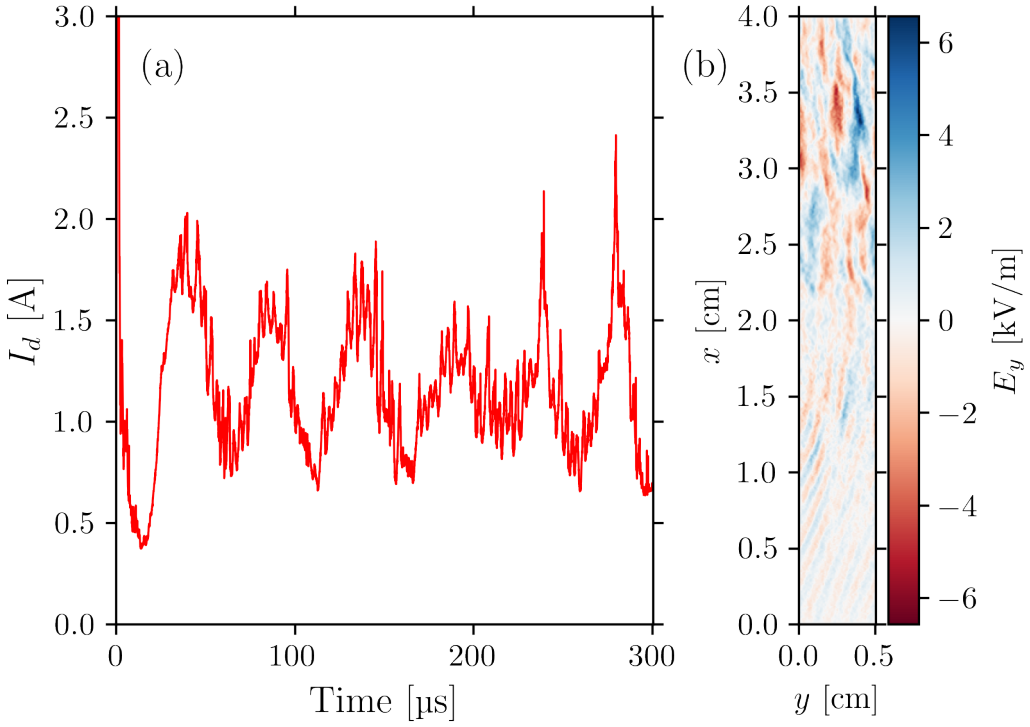

Figure 2. Subfigure (a) shows the discharge current evolution over time, while subfigure (b) shows a snapshot at $t = 200\,\mu s$ of the azimuthal electric field.

described with 1D Euler equations coupled to the PIC/MCC. The description of this code has already been given in several articles.[13,27–30] In the following, we will discuss only its main features.

In Fig. 1(a), we present a simplified scheme of the simulation domain. The spatial domain consists of a Cartesian mesh with periodic boundary conditions along the azimuthal (y) direction. The boundaries in the x direction are defined by the anode and the cathode, with the cathode grounded. Electrons are injected at each time step to maintain quasi-neutrality in the last cell. The anode, at high voltage, is controlled by an external circuit as shown in Fig. 1(b) and discussed in Ref. 29. A constant out-of-plane magnetic field is applied to recreate the $\mathbf{E} \times \mathbf{B}$ drift of electrons. A snapshot of the electric field and the discharge current is shown in Fig. 2(b).

The neutral dynamics are solved using 1D Euler equations along the x direction with an HLLC solver.[31] A fixed neutral flux rate is imposed at the anode, while the cathode boundary has open boundary conditions. The 1D Euler system in LPPic is:

$$\begin{cases} \partial_t \rho_g + \partial_x(\rho_g u_g) & = S_1, \\ \partial_t(\rho_g u_g) + \partial_x(\rho_g u_g^2) & = -\partial_x P_g + S_2. \end{cases}$$

Here, ρ_g is the neutral density, u_g is the neutral fluid velocity, S_1 and S_2 are collisional source terms, and P_g is the neutral pressure. The neutral gas temperature is set to 640 K. More details are provided in Charoy *et al.*[13] A constant mass flow of neutral gas is injected at the anode, accounting for neutrals produced from ion recombination. The equations deal with a flux $\Gamma_g = \rho_g u_g$, requiring the definition of the device area to obtain the real mass flow rate.

In real HT devices, the radial dimension influences plasma characteristics. Inside the channel, particles leave via Bohm flux at the grounded walls. Outside, the plume dynamics exhibit a high divergence angle.[32] Since LPPic is a 2.5D code, radial dynamics has been modeled indirectly via a virtual radial direction, as detailed in Refs. 30, 33.

To relax numerical constraints, a permittivity scaling factor of 16 was used. It allows to increase the time step and mesh size by a factor of 4. Despite potential effects on plasma dynamics, this scaling does not significantly impact the quasi-stationary state. A comprehensive list of simulation parameters, inspired by those of the PPS1350 by Safran, is provided in Table 1.

The discharge current measured in the simulation, see Fig. 2(a), shows a rather standard behavior for this kind of discharge: we can clearly distinguish the kHz breathing mode (BM) oscillations superimposed to higher frequency modulation. In Fig. 2(b), one can observe a snapshot of the azimuthal electric field. The anode is at $x = 0$ cm, while the cathode is at $x = 4$ cm. The electric field oscillations are larger at the cathode, as expected. We can recognize the usual pattern of the azimuthal electric field oscillations, which are related to the Electron Cyclotron Drift Instability (ECDI).[34]

IV. Results from the hybrid simulation

In this section, we will challenge the assumptions taken in the analytical model by using the results of the simulation described in Section III.

In Fig. 3 we show some axial (along x) profiles of plasma quantities, averaged azimuthally and in time (i.e., between 150 and 300 µs). As one can see in Fig. 3(a), the electron axial velocity is low in the plume. As the electrons approach the anode, their speed increases. In Fig. 3(b), we show the electric field and the pressure gradient. The electric field is significantly larger than the pressure gradient. However, the pressure gradient is not negligible. Both these quantities are low near the anode and in the plume, with a maximum near the channel exit. In Fig. 3(c), we show the cyclotron frequencies and the collision frequencies, extracted from the simulation results. One can notice that the cyclotron frequency, in these conditions, is always larger than the collision frequency. This consideration justifies the approximation of the electron collisional mobility in Eq. (6).

The elastic and excitation collision frequencies are particularly high near the anode. The reason of that is related to the high neutral density at the channel entrance. The ionization frequency, on the contrary, is larger at the channel exit. The reason for that is related to the larger electron temperature in that region. In Fig. 3(d), we show the collisional mobility and the mobility obtained by reverting Eq. (5) and neglecting the drift terms. The two mobilities are rather similar inside the channel region, while they differ in the plume. The mobility difference that is still persistent inside the channel can be related to the wall-collision,

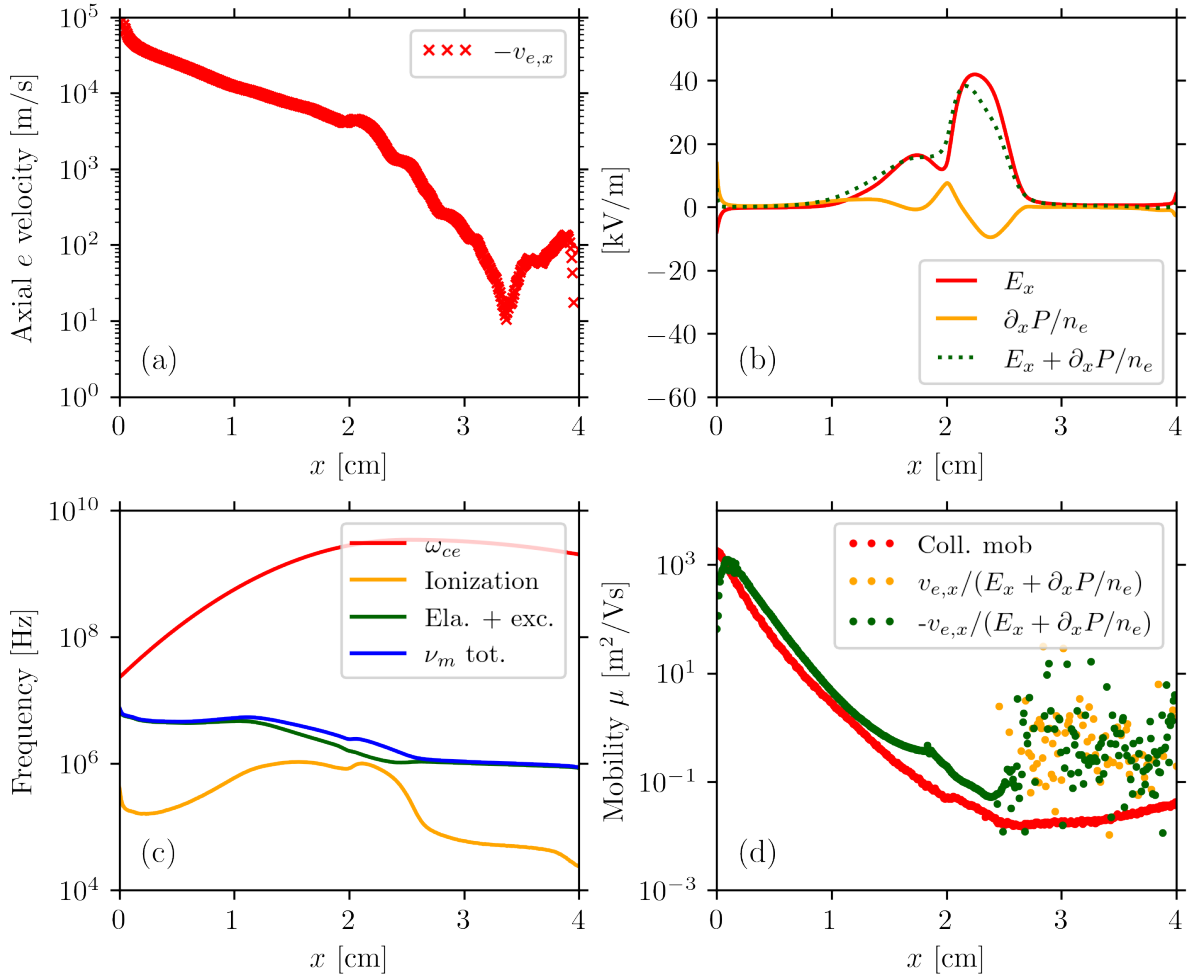

Figure 3. (a) Axial electron velocity, (b) electric field and pressure gradient, (c) collision frequencies and cyclotron frequencies profile, and (d) collisional mobility and mobility from the simulation.

as suggested by Morozov.[35] In the plume, the collisional mobility is underestimating the actual one by one or two orders of magnitude. This is in good agreement with the remarks about the anomalous transport well-known in the literature.[2]

A. Electron azimuthal transport

To understand the approximations made in Section II, we study in detail the different terms of Eq. (5) in both azimuthal and axial direction. In Fig. 4 we show the azimuthal electron velocity and its components. The time is fixed to $t = 150\,\mu s$. In (a) we show the azimuthal electron drift calculated as in Eq. (7). In (b) we show the azimuthal diamagnetic drift calculated as in Eq. (8). The sum of these two is reported in (c). One can notice that it is almost equal to the azimuthal electron velocity directly extracted from the simulation results (d). When we do an azimuthal average of the profiles, we obtain the results shown in (e). As one can see, the sum of $\mathbf{E} \times \mathbf{B}$ and diamagnetic drift perfectly reproduces the actual azimuthal electron velocity.

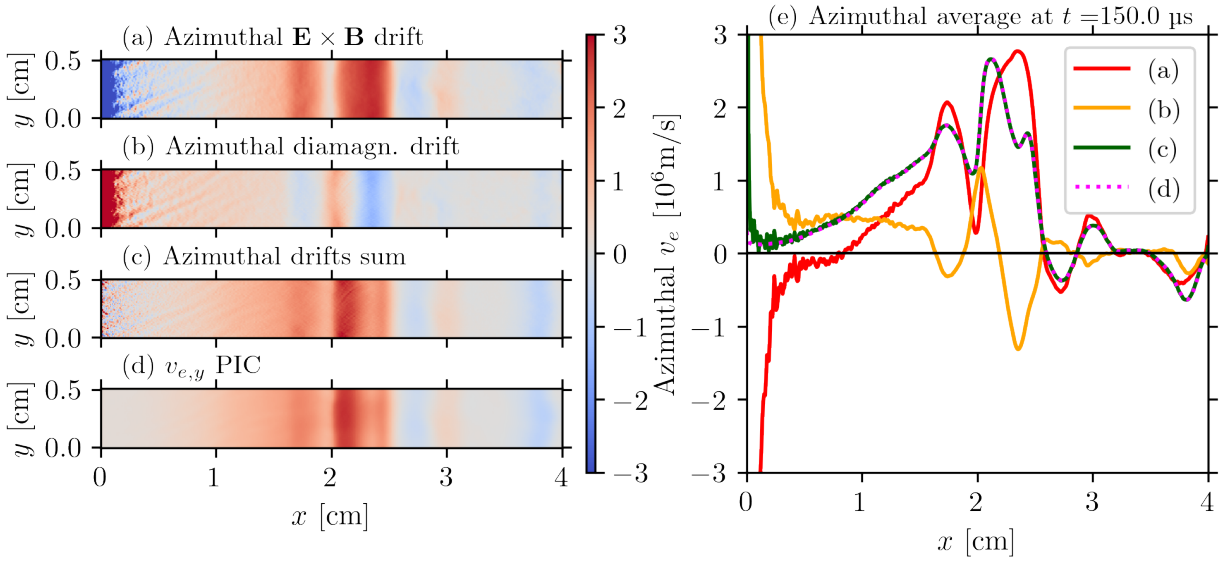

Figure 4. Analysis of the electron velocity in the azimuthal direction at $t = 150\,\mu s$. Snapshots of (a) Azimuthal $\mathbf{E} \times \mathbf{B}$ drift, (b) azimuthal diamagnetic drift, (c) drifts sum, and (d) azimuthal electron velocity from the hybrid simulation. (e) Azimuthally averaged profiles of the snapshots. The legend in (e) refers to the snapshots in the left column.

The results in Fig. 4 highlight the fact that the azimuthal motion of the electrons is dominated by the $\mathbf{E} \times \mathbf{B}$ and diamagnetic drifts. The collisional mobility terms, i.e. the first two terms of Eq. (5), along the y direction are negligible.

B. Electron axial transport

When we try to do the same exercise for the axial component of the electron speed, the exercise becomes more complicated. In Fig. 5 we show the axial electron velocity and its components. As we have highlighted in Fig. 3(d), the electron axial motion inside the thruster channel is dominated by the collisional mobility. On the contrary, in the plume region, the motion is largely dominated by drift-related terms. Figures 5(a) and (b) show the axial velocity induced by $\mathbf{E} \times \mathbf{B}$ and diamagnetic drifts, respectively. Their sum is shown in Fig. 5(d). The collisional mobility contribution to the axial velocity is shown in Fig. 5(c). As one can see in Fig. 5(e), the sum of the drifts allows the actual axial velocity of electrons to be reproduced conveniently.

In Fig. 5(f) we show the different axial velocity components at a fixed azimuthal position in the plume. We highlight that this quantity is not an azimuthal average. From this figure, it is clear how the fluctuations of the electric field and of the pressure gradient in the azimuthal direction are the only contributors to the

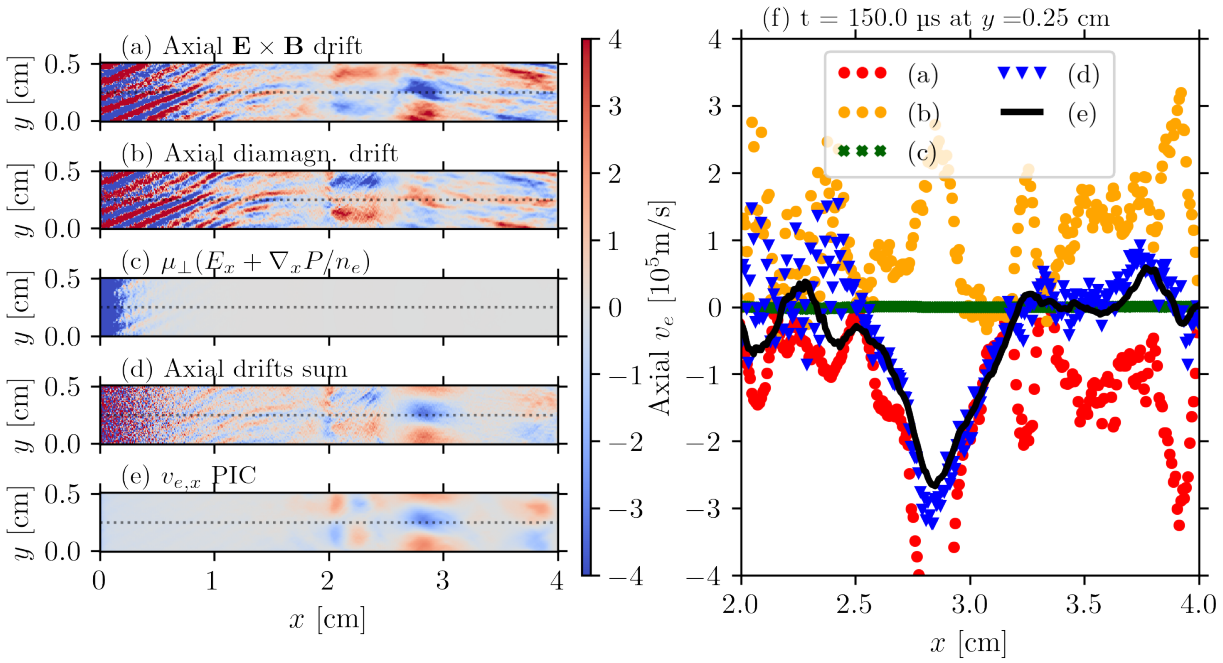

Figure 5. Analysis of the electron velocity in the axial direction at $t = 150\,\mu s$. Snapshots of (a) Axial $\mathbf{E}\times\mathbf{B}$ drift, (b) axial diamagnetic drift, (c) collisional mobility contribution, (d) drifts sum, and (e) axial electron velocity from the hybrid simulation. (f) Axial profiles of the snapshots at $y = 0.25\,cm$. The legend in (f) refers to the snapshots in the left column.

axial electron transport in the thruster plume. The collisional mobility (in green in the figure) is negligible in the plume.

If we want to evaluate the approximation in Eq. (13), we have to look at the azimuthal average of electron fluxes profiles. In Fig. 6 we show the azimuthal average of the electron flux components at different times. From the red and yellow curves, we can notice that the approximation $\langle nE_y\rangle_y = \langle \delta n \delta E_y\rangle_y$ is reasonable. Moreover, we notice that the diamagnetic drift averages to zero most of the time (green curve). However, when we sum the two drifts (blue curve), it weakly approaches the actual azimuthally averaged electron axial velocity (black curve).

The origin of this discrepancy is related to the relative stiffness of the averaging operation. The instability wave propagates in the azimuthal direction, and, as one can see in Fig. 5, the axial velocity components are such that

$$\sqrt{\langle v_{e,y}^2\rangle_y} \gg \langle v_{e,y}\rangle_y.$$

For this reason, when we perform the azimuthal average of the flux components the result shows a significant amount of noise.

To overcome this issue, we can leverage the almost-purely azimuthal origin of the plume instability. In Fig. 7 we show the components of the axial electron flux at $t = 150\,\mu s$. The subfigures (a), (b), (c), and (d) show the same quantities as in Fig. 5. Subfigure (f) represents a novelty. We show here the axial average of the flux components between $x = 2.5\,cm$ and $x = 4\,cm$ (i.e., the patterned region on the left column's snapshots). As one can see, the sum of the drifts is almost equal to the actual axially averaged axial electron velocity.

The operation of doing an axial average somehow reduces the stiffness of the problem. Then we can proceed to the azimuthal average of the flux components. In Fig. 8 we show the temporal evolution of the total spatial average of the electron flux components. As one can see, the diamagnetic drift flux has a rather low effect on electron transport. The same conclusion can be drawn for the collisional transport. The $\mathbf{E}\times\mathbf{B}$ drift flux is the main contributor to the electron transport in the axial direction in the plume. Even though some differences persist, the time averages of these quantities (e.g. $\langle \mathbf{E}\times\mathbf{B}\text{ drift}\rangle_t \approx -8.84\times10^{19}\,m^{-2}s^{-1}$ and $\langle \text{PIC axial } e \text{ flux}\rangle_t \approx -7.65\times10^{19}\,m^{-2}s^{-1}$) are very close to each other.

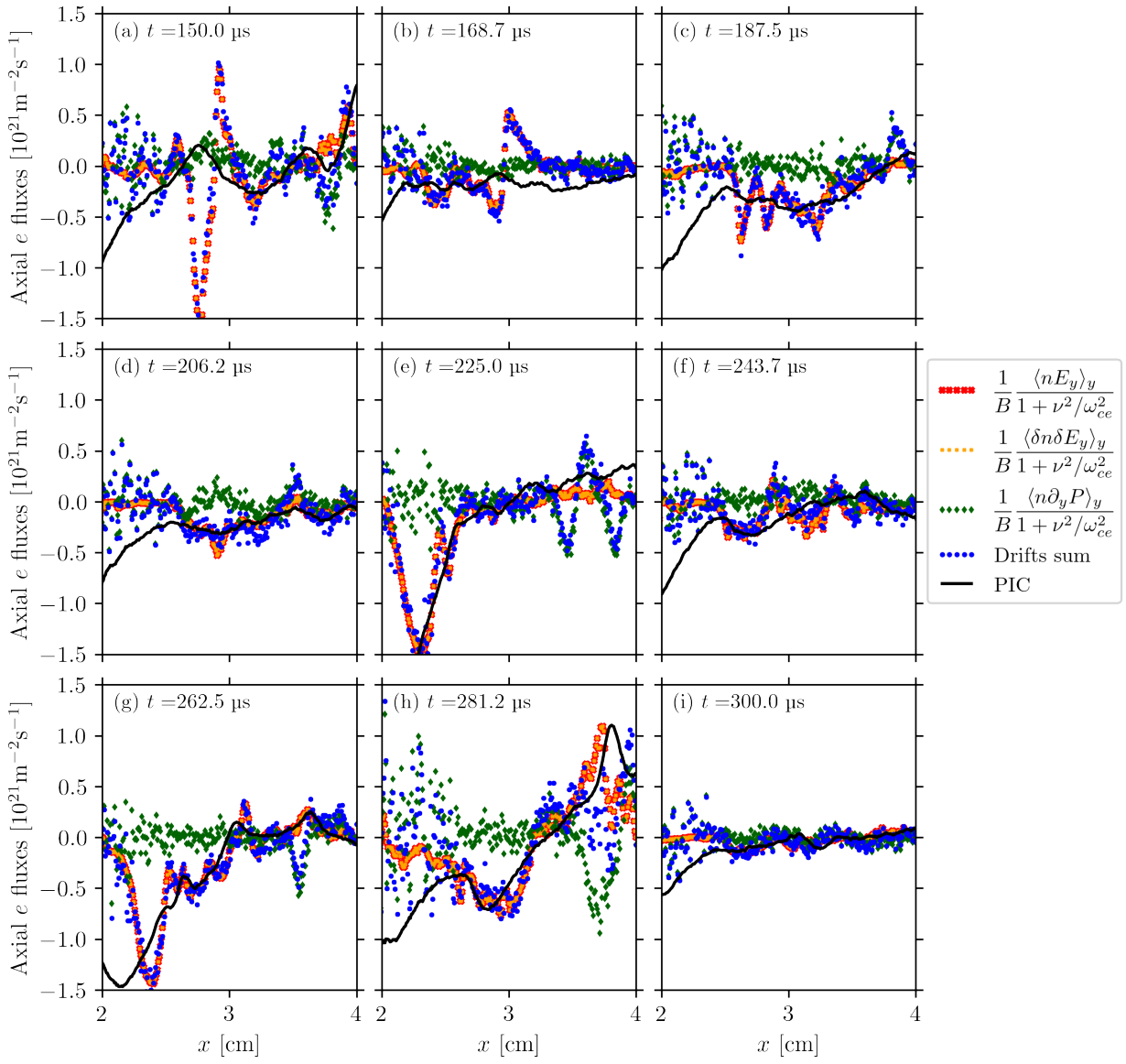

Figure 6. Axial (azimuthally averaged) electron fluxes profiles at different times. The legend lists the different flux components.

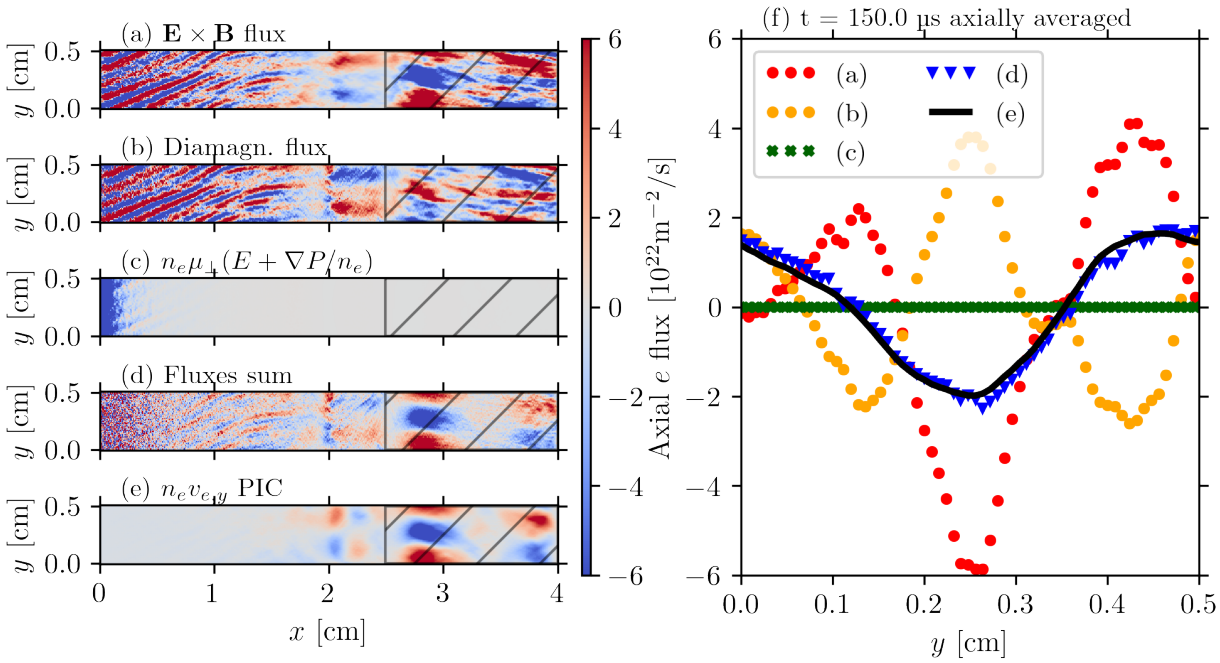

Figure 7. Analysis of the electron velocity in the axial direction at $t = 150\,\mu s$. Snapshots of (a) Axial $\mathbf{E}\times\mathbf{B}$ drift, (b) axial diamagnetic drift, (c) collisional mobility contribution, (d) drifts sum, and (e) axial electron velocity from the hybrid simulation. (f) Azimuthal profiles of the snapshots averaged axially between 2.5 and 4 cm (i.e. see the pattern on the left column). The legend in (f) refers to the snapshots in the left column.

From the results in Fig. 8 we can conclude that the approximation in Eq. (13) is reasonable. The azimuthal average of the electron flux components can be approximated by the correlation of the fluctuations of the electron density and the azimuthal electric field. Although important at a fixed y, the effect of the diamagnetic drift averages to zero and should be neglected when considering only the axial transport of electrons in the plume, as in a 1D fluid model.

V. Insights from 1D fluid simulation

In this section, we discuss some preliminary results obtained from 1D fluid simulations. The fluid simulation resolves the quasi-neutral system (1), (2), (3), and (4). The numerical scheme uses finite volumes with a third-order Runge-Kutta time integration.[36] The model is similar to the one of Refs.,[22,23] both inspired by Barral and Ahedo work.[16]

The major difference compared to these works is that we use the Ψ-flux introduced in Section II and expressed in Eq. (13). The Ψ-flux is here case set to a non-null value in the plume and is set to zero in the channel. The value of $\langle n\Psi_x\rangle_y$ is set to $500n\beta$, with β of the order of the unity. This value is reasonable when compared to the results of the hybrid simulations in Section III. In order to favour the model convergence, we set a constant background collision frequency of $8.79\times10^6\,\mathrm{s}^{-1}$ all along the simulation axis.

As one can observe in Fig. 9(a), the Ψ-flux is set constant in the plume and zero in the channel and near the cathode. Some linear smoothing of the profile is used to avoid sharp changes in the Ψ-flux value. The discharge currents time evolution are shown in Fig. 9 for different values of the parameter β. The results show that the discharge current is affected by the value of β, so by the presence of the Ψ-flux in the simulation.

By extracting the plasma parameters from the system, one obtains the results shown in Fig. 10. We can notice that the neutral density in the plume is strongly affected by the variation of the parameter β. Consistently with that, the plasma density also varies: when β is negative, we observe a plasma accumulation outside the channel. The electron temperature increases at the thruster exit when β is negative, while it slightly decreases when β is positive. The ion axial variation does not seem to vary significantly when we

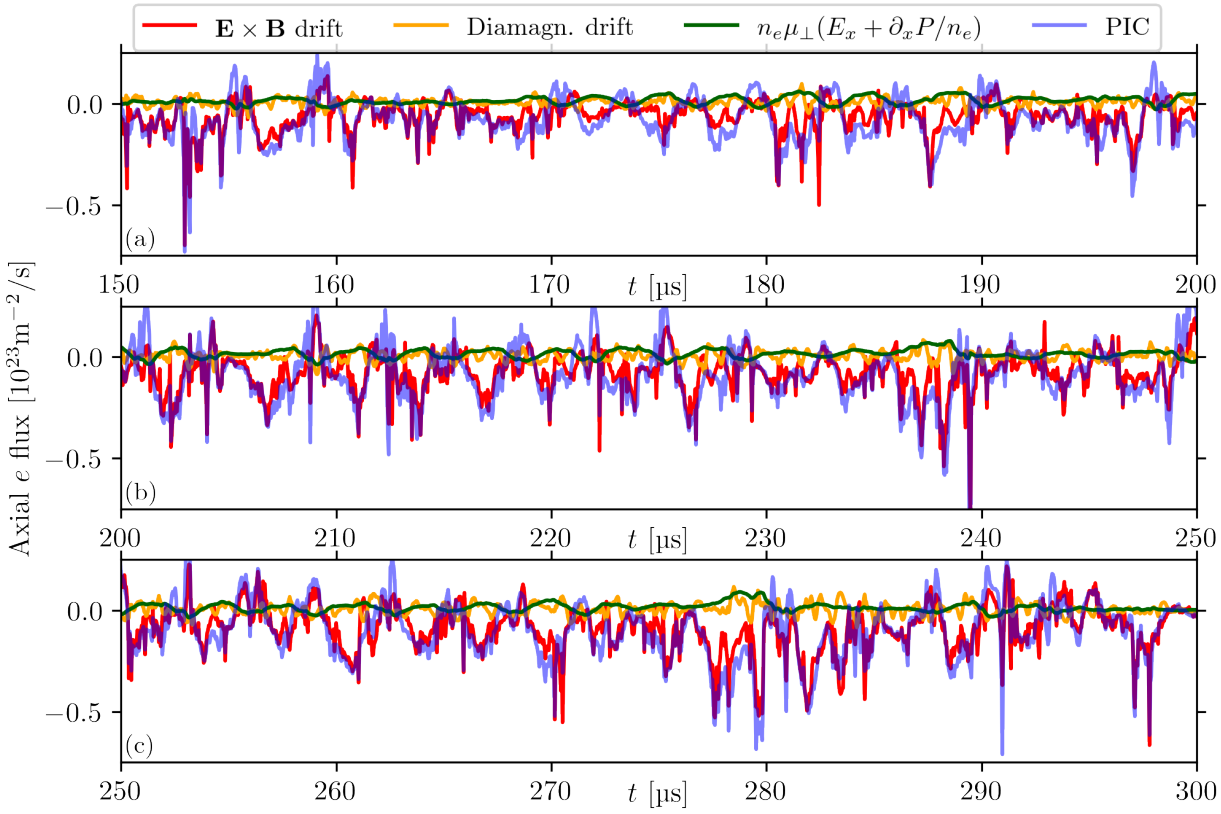

Figure 8. Temporal evolution of the mean axial electron flux components in the plume. The time axe is split into three subfigures to ease the reading.

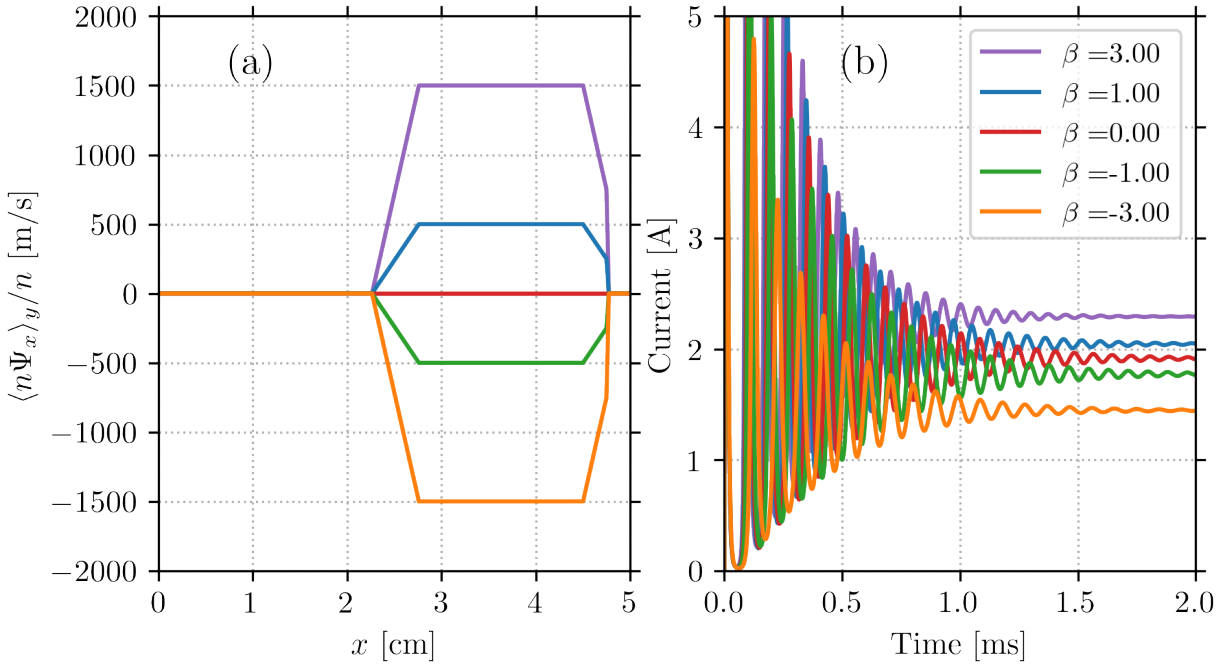

Figure 9. Fluid simulation results. (a) Axial profiles of the *Psi*-velocity. (b) Temporal evolution of the discharge current.

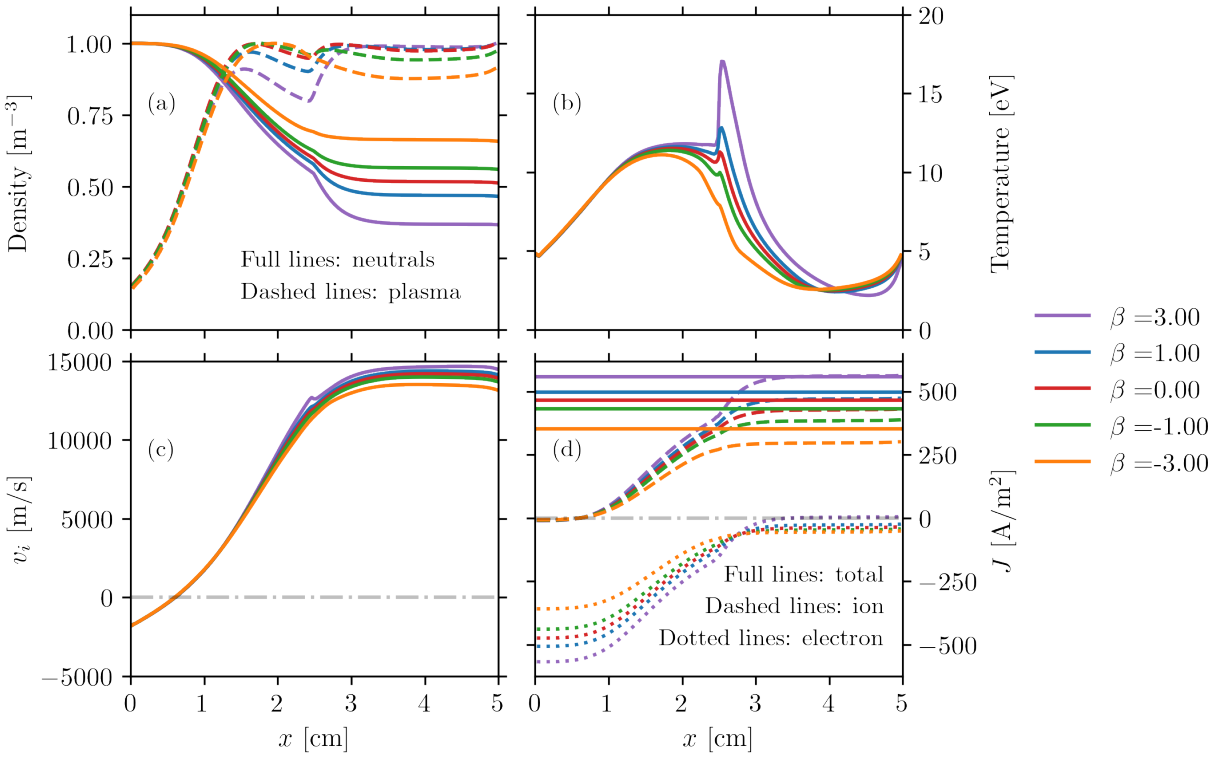

Figure 10. Fluid simulation results. (a) Normalized neutral (full lines) and plasma (dashed lines), (b) electron temperature, (c) ion axial velocity, and (d) Axial current density, for different values of the parameter β.

vary β. However, the total current does, as we have seen previously in Fig. 9(b). By computing the electron and ion contributions to the current density, we can see that the electron current remains substantially unchanged in the plume, while it varies importantly in the channel. The ion current, on the contrary, is almost unaffected in the channel and varies in the plume.

VI. Conclusions and perspectives

In this work, we first developed a theory to account for the anomalous transport in fluid equations starting from textbook fluid theory. We derive a velocity term depending on the electric field and the density fluctuations, and we have shown how this velocity should be used in the fluid models.

Subsequently, we verified the assumptions made in the theory by using a hybrid simulation. We showed that the azimuthal electron transport is dominated by the $\mathbf{E} \times \mathbf{B}$ and diamagnetic drifts, while the collisional mobility is negligible in the plume. The azimuthal average of the electron flux components can be approximated by the correlation of the fluctuations of the electron density and the azimuthal electric field. The diamagnetic drift, which is important when we consider a single azimuthal position, averages (in the azimuthal direction) to zero. We deduced that it should be neglected when considering only the axial transport of electrons in the plume, as in a 1D fluid model.

In the last part of the work, we showed some preliminary results from 1D fluid simulations. We introduced the Ψ-flux in the fluid equations and we showed how the plasma parameters are affected by the presence of this velocity. We showed that the discharge current is affected by the value of the parameter β, so by the presence of the Ψ-flux in the simulation. Even though these results are promising, we still need to use a constant background collision frequency to favour the model convergence.

The model is still in a preliminary stage, yet, the Ψ-flux seems to be a good candidate to account for the anomalous transport in fluid equations. The next steps will be to improve the model by introducing a more realistic space and time-varying profile of this quantity.

Table 1. Operating and numerical parameters used in the hybrid simulations.

Physical parameters	Symbol	Value	Unit
Gas		Xenon	(-)
Radial magnetic field (max)	B	170	G
Imposed voltage	V_a	300	V
Cathode voltage	V_c	0	V
Axial length	L_x	4	cm
Azimuthal length	L_y	0.512	cm
Radial length	L_z	1.55	cm
Initial plasma density	n_0	5×10^{18}	m^{-3}
Initial electron temperature	T_e	1	eV
Initial ion temperature	T_i	0.05	eV
Neutral mass flow rate	$\dot{m}$	5	$\mathrm{mg\,s}^{-1}$
Thruster section	Area	3.768×10^{-3}	m^2
Cathode injection temperature	T_e^{cath}	5	eV
Resistance	R	60	Ω
Inductance	L	4.4	mH
Capacitance	C	15	nF
Simulation parameters			
Time step	Δt	8×10^{-12}	s
Cell size	$\Delta x = \Delta y$	8×10^{-5}	m
Number of cells	$x_{\max} \times y_{\max}$	500×63	(-)
Initial number of particles per cell	N/NG	400	particles/cell
Macro-particles weight factor	q_f	1.6×10^7	m^{-1}
Number of iterations between outputs	N_a	5000	(-)
Permittivity scaling	α^0	16	(-)

Acknowledgments

The work was partially supported by Agence de l'Innovation de Défense – AID - via Centre Interdisciplinaire d'Etudes pour la Défense et la Sécurité – CIEDS - (project 2023 – validHETion). The work was granted access to the HPC resources of TGCC under the allocations A0100510439, A0120510439, and A0140510439 made by GENCI.

Data Availability

The data that support the findings of this study are available from the corresponding author upon reasonable request.

References

[1]I. D. Kaganovich, A. Smolyakov, Y. Raitses, E. Ahedo, I. G. Mikellides, B. Jorns, F. Taccogna, R. Gueroult, S. Tsikata, A. Bourdon, J.-P. Boeuf, M. Keidar, A. T. Powis, M. Merino, M. Cappelli, K. Hara, J. A. Carlsson, N. J. Fisch, P. Chabert, I. Schweigert, T. Lafleur, K. Matyash, A. V. Khrabrov, R. W. Boswell, and A. Fruchtman. Physics of E × B discharges relevant to plasma propulsion and similar technologies. *Physics of Plasmas*, 27(12):120601, December 2020.

[2]J C Adam, J.-P. Boeuf, N Dubuit, M Dudeck, D Garrigues, L.and Gresillon, A Heron, G J M Hagelaar, V Kulaev, N Lemoine, S Mazouffre, J Perez Luna, V Pisarev, and S Tsikata. Physics, simulation and diagnostics of Hall effect thrusters. *Plasma Physics and Controlled Fusion*, 50(12):124041, December 2008.

[3]K. Komurasaki and Y. Arakawa. Two-dimensional numerical model of plasma flow in a Hall thruster. *Journal of Propulsion and Power*, 11(6):1317–1323, November 1995.

[4]J.-P. Boeuf and L Garrigues. Low frequency oscillations in a stationary plasma thruster. *Journal of Applied Physics*, 84(7):3541–3554, 1998.

[5]J. M. Fife. *Hybrid-PIC Modeling and Electrostatic Probe Survey of Hall Thrusters*. PhD thesis, Massachusetts Institute of Technology, February 1999.

[6]G. J. M. Hagelaar, J. Bareilles, L. Garrigues, and J.-P. Boeuf. Role of anomalous electron transport in a stationary plasma thruster simulation. *Journal of Applied Physics*, 93(1):67–75, January 2003.

[7]J. Cavalier, N. Lemoine, G. Bonhomme, S. Tsikata, C. Honoré, and D. Grésillon. Hall thruster plasma fluctuations identified as the E×B electron drift instability: Modeling and fitting on experimental data. *Physics of Plasmas*, 20(8):082107, August 2013.

[8]T. Lafleur, S. D. Baalrud, and P. Chabert. Theory for the anomalous electron transport in Hall effect thrusters. I. Insights from particle-in-cell simulations. *Physics of Plasmas*, 23(5):053502, May 2016.

[9]T. Lafleur, S. D. Baalrud, and P. Chabert. Theory for the anomalous electron transport in Hall effect thrusters. II. Kinetic model. *Physics of Plasmas*, 23(5):053503, May 2016.

[10]T. Lafleur and P. Chabert. The role of instability-enhanced friction on 'anomalous' electron and ion transport in Hall-effect thrusters. *Plasma Sources Science and Technology*, 27(1):015003, December 2017.

[11]J. C. Adam, A. Héron, and G. Laval. Study of stationary plasma thrusters using two-dimensional fully kinetic simulations. *Phys. Plasmas*, 11(1):12, 2004.

[12]T. Lafleur, R. Martorelli, P. Chabert, and A. Bourdon. Anomalous electron transport in Hall-effect thrusters: Comparison between quasi-linear kinetic theory and particle-in-cell simulations. *Physics of Plasmas*, 25(6):061202, June 2018.

[13]T. Charoy, T. Lafleur, A. Alvarez Laguna, A. Bourdon, and P. Chabert. The interaction between ion transit-time and electron drift instabilities and their effect on anomalous electron transport in Hall thrusters. *Plasma Sources Science and Technology*, 30(6):065017, June 2021.

[14]T. A. Marks and B. A. Jorns. Evaluation of algebraic models of anomalous transport in a multi-fluid Hall thruster code. *Journal of Applied Physics*, 134(15):153301, October 2023.

[15]J. W. Koo and I. D. Boyd. Modeling of anomalous electron mobility in Hall thrusters. *Physics of Plasmas*, 13(3):033501, March 2006.

[16]S. Barral and E. Ahedo. Low-frequency model of breathing oscillations in Hall discharges. *Physical Review E*, 79(4):046401, April 2009.

[17]K. Kwon, M. L. R. Walker, and D. N. Mavris. Self-consistent, one-dimensional analysis of the Hall effect thruster. *Plasma Sources Science and Technology*, 20(4):045021, August 2011.

[18]K. Hara and I. G. Mikellides. Characterization of low frequency ionization oscillations in Hall thrusters using a one-dimensional fluid model. In *AIAA Propulsion and Energy Forum*, 2018.

[19]I. G. Mikellides and A. Lopez Ortega. Challenges in the development and verification of first-principles models in Hall-effect thruster simulations that are based on anomalous resistivity and generalized Ohm's law. *Plasma Sources Science and Technology*, 28(1):014003, January 2019.

[20]V. Giannetti, M. Martín Saravia, L. Leporini, S. Camarri, and T. Andreussi. Numerical and Experimental Investigation of Longitudinal Oscillations in Hall Thrusters. *Aerospace*, 8(6):148, May 2021.

[21]D. Poli, E. Bello-Benítez, P. Fajardo, and E. Ahedo. Time-dependent axial fluid model of the Hall thruster discharge and its plume. *Journal of Physics D: Applied Physics*, 56(41):415203, October 2023.

[22]R. Martorelli, T. Lafleur, A. Bourdon, and P. Chabert. Comparison between ad-hoc and instability-induced electron anomalous transport in a 1d fluid simulation of hall-effect thruster. *Physics of Plasmas*, 26(8):083502, 2019.

[23]T. Lafleur, P. Chabert, and A. Bourdon. The origin of the breathing mode in Hall thrusters and its stabilization. *Journal of Applied Physics*, 130(5):053305, August 2021.

[24]M. A. Lieberman and A. J. Lichtenberg. *Principles of plasma discharges and materials processing*. John Wiley & Sons, 2005.

[25]T. Charoy, J.-P. Boeuf, A. Bourdon, J. A. Carlsson, P. Chabert, B. Cuenot, D. Eremin, L. Garrigues, K. Hara, I. D. Kaganovich, A. T. Powis, A. Smolyakov, D. Sydorenko, A. Tavant, O. Vermorel, and W. Villafana. 2D axial-azimuthal particle-in-cell benchmark for low-temperature partially magnetized plasmas. *Plasma Sources Science and Technology*, 28(10):105010, October 2019.

[26]W. Villafana, F. Petronio, A C. Denig, M J. Jimenez, D. Eremin, F. Garrigues, L.and Taccogna, A. Alvarez-Laguna, J.-P.. Boeuf, A. Bourdon, P. Chabert, T. Charoy, B. Cuenot, K. Hara, F. Pechereau, A. Smolyakov, D. Sydorenko, A. Tavant, and O Vermorel. 2D radial-azimuthal particle-in-cell benchmark for E × B discharges. *Plasma Sources Science and Technology*, 30(7):075002, July 2021.

[27]V. Croes, T. Lafleur, Z. Bonaventura, A. Bourdon, and P. Chabert. 2D particle-in-cell simulations of the electron drift instability and associated anomalous electron transport in Hall-effect thrusters. *Plasma Sources Science and Technology*, 26(3):034001, February 2017.

[28]T. Charoy, T. Lafleur, A. Tavant, P. Chabert, and A. Bourdon. A comparison between kinetic theory and particle-in-cell simulations of anomalous electron transport in E × B plasma discharges. *Physics of Plasmas*, 27(6):063510, June 2020.

[29]F. Petronio, T. Charoy, A. Alvarez Laguna, A. Bourdon, and P. Chabert. Two-dimensional effects on electrostatic instabilities in hall thrusters. i. insights from particle-in-cell simulations and two-point power spectral density reconstruction techniques. *Physics of Plasmas*, 30(1):012103, 01 2023.

[30]F. Petronio, A. Alvarez Laguna, A.and Bourdon, and P. Chabert. Study of the breathing mode development in Hall thrusters using hybrid simulations. *Journal of Applied Physics*, 135(7):073301, 02 2024.

[31]E. F. Toro. *Riemann solvers and numerical methods for fluid dynamics: a practical introduction*. Springer-Verlag, Berlin; New York, 2nd ed edition, 1999.

[32]Z. Zhang, Z. Zhang, H. Tang, W. Yeong Liang Ling, Z. Chen, J. Ren, and J. Cao. Measurement of the distribution of charge exchange ions in a hall-effect thruster plume. *Plasma Sources Science and Technology*, 29(8):085001, 2020.

[33]F. Petronio, A. Alvarez Laguna, A.and Bourdon, and P. Chabert. The introduction of a virtual radial direction in axial-azimuthal PIC simulations of Hall Thrusters. In *37th International Electric Propulsion Conference*, Boston, Massachussets, June 2022.

[34]F. Petronio, T. Charoy, A. Alvarez Laguna, A.and Bourdon, and P. Chabert. Two-dimensional effects on electrostatic instabilities in hall thrusters. ii. comparison of particle-in-cell simulation results with linear theory dispersion relations. *Physics of Plasmas*, 30(1):012104, 01 2023.

[35]A.I. Morozov. Wall conduction in a highly magnetized plasma. *Journal of Applied Mechanics and Technical Physics*, 9(3):249–251, 1968.

[36]S. Gottlieb and C.-W. Shu. Total variation diminishing runge-kutta schemes. *Mathematics of computation*, 67(221):73–85, 1998.